Commun. Theor. Phys. (Beijing, China) **54** (2010) pp. 359–364

Vol. 54, No. 2, August 15, 2010

Electron Acceleration and Bunch Generation by Intense Femtosecond Laser Pulse in Preplasma of a Target*

LIU Ming-Ping (刘明萍),[1,†] WANG Qing-Nian (汪庆年),[1] DENG Su-Hui (邓素辉),[2] LIU San-Qiu (刘三秋),[3] and XIE Bai-Song (谢柏松)[4]

[1]College of Information Engineering, Nanchang University, Nanchang 330031, China

[2]Laboratory of Physical Biology, Shanghai Institute of Applied Physics, Chinese Academy of Sciences, Shanghai 201800, China

[3]Department of Physics, Nanchang University, Nanchang 330047, China

[4]College of Nuclear Science and Technology, Beijing Normal University, Beijing 100875, China

(Received October 19, 2009)

Abstract *We present analytical studies of electron acceleration in the low-density preplasma of a thin solid target by an intense femtosecond laser pulse. Electrons in the preplasma are trapped and accelerated by the ponderomotive force as well as the wake field. Two-dimensional particle-in-cell simulations show that when the laser pulse is stopped by the target, electrons trapped in the laser pules can be extracted and move forward inertially. The energetic electron bunch in the bubble is unaffected by the reflected pulse and passes through the target with small energy spread and emittance. There is an optimal preplasma density for the generation of the monoenergetic electron bunch if a laser pulse is given. The maximum electron energy is inverse proportion to the preplasma density.*

PACS numbers: 52.38.-r, 52.38.Kd, 52.25.Dg, 52.65.Rr
Key words: femtosecond laser-plasma interaction, electron acceleration, monoenergetic electron bunch, PIC simulation

1 Introduction

Laser-driven electron acceleration has received great attention because of its mangy potential applications, such as in compact accelerators,[1−2] x-ray generation,[3] fast ignition in inertial confinement fusion,[4] etc., and much work in this area has appeared in the literature.[5−10] It is known that a plane-wave laser pulse cannot be used for electron acceleration. Since when a wave overtakes an electron, the radiation pressure pushes the electron forward in the rising part and backward in the trailing part of the laser pulse. As a result, the electron gains no net energy. In order to avoid the decelerating phase, it has been proposed[11−12] that the laser pulse be stopped by a thin solid target, so that the accelerated electrons in the pulse front can avoid the deceleration phase and move forward inertially and pass through the target with little energy loss if their stopping distance is much larger than the target thickness. The electron energy at the peak of the propagating pulse scales as the laser intensity I, which is much higher than that (scaling as $\sqrt{I}$) from the laser-target interactions.

Rapid development of laser technology has made available ultraintense ($I\lambda^2 > 1 \times 10^{18}$ W cm$^{-2}\mu$m^2, where λ is the wavelength) femtosecond laser pulse. Such laser pulse interactions with plasma has opened a gate to the new concept of particle accelerators. One of the promising schemes is the laser wake field acceleration (LWFA) in a new, highly non-linear bubble regime, which appears as a nearly electron free bubble in two or three dimensions.[13−17] Electrons that remain or enter the bubble will be trapped and accelerated to a high energy by the extremely strong electrostatic field on its backside node. The resulting electron bunch is quasimonoenergetic and has a narrow spread. It has been shown in recent experiments[18−20] that self-injected electrons can be accelerated to almost the same energy, leading to monoenergetic electrons beams. Note that the formation of the bubble depends greatly on the parameters of the pulse and plasma.[21] For example, The laser intensity must be high enough and pulse duration must be short enough. The plasma density must also be large enough for the laser pulse to self-focus and small enough for the plasma wavelength to be comparable to the pulse duration.

In laser-target experiments,[22] there is generally a prepulse before the main pulse, and the time interval of them is typically a few picoseconds/nanoseconds. The intensity of the prepulse is so strong to ionize the target and leads to the formation of low-density preplasma at the front of the target before the arrival of the main pulse. In this paper we investigate electron acceleration in the interaction of an intense femtosecond laser pulse with a preplasma and extraction of the energetic electrons by a solid target.

*Supported by the National Natural Science Foundation of China under Grant Nos. 10875015, 10834008, 10963002 and partially by the 973 Program under Grant No. 2006CB806004, and by Educational Commission of Jiangxi Province of China under Grant No. GJJ10052
†Correspondence author, E-mail: mpliu2008@gmail.com

The electrons in the preplasma can be trapped and accelerated forward by the ponderomotive force as well as the wake bubble. Particle-in-cell (PIC) simulations show that when the laser pulse is reflected by the target,[11−12] the energetic electron bunch in the bubble is unaffected by the reflected pulse and can propagate through the thin target with little energy loss and spread. The effect of preplasma densities on the electron acceleration and bunch generation is also investigated, and there is an optimal preplasma density for the generation of the monoenergetic electron bunch.

2 Model of Electron Acceleration

2.1 *Formulation*

We first consider the acceleration of electrons by the plane-wave laser pulse and its wake field in terms of a simple one-dimensional (1D) analytical model. The Hamiltonian for the relativistic motion of an electron in an electromagnetic field is[17,23]

$$H(x,t,\mathbf{P}) = \sqrt{m^2c^4 + (\mathbf{P}c + e\mathbf{A})^2} - e\phi\,, \qquad (1)$$

where $\mathbf{P} = \mathbf{p} - e\mathbf{A}/c$ is the canonical momentum, $\mathbf{p}$ is the electron momentum, $\mathbf{A}$ is the vector potential of the laser pulse, ϕ is the electrostatic potential of the wakefield, c is the light speed in vacuum, m and $-e$ are the mass and charge of the electron, respectively. It is convenient to use dimensionless variables, i.e., $\mathbf{P} = \mathbf{P}/mc$, $\mathbf{p} = \mathbf{p}/mc$, $\mathbf{a} = e\mathbf{A}/mc^2$, $\phi = e\phi/mc^2$, and $H = H/mc^2$. Then the normalized Hamiltonian is

$$H(x,t,\mathbf{P}) = \sqrt{1 + (\mathbf{P} + \mathbf{a})^2} - \phi\,. \qquad (2)$$

Since the background plasma density is low for LWFA, the dispersion of the short laser pulse during the interaction can be negligible. $\mathbf{a}$ and ϕ then depend on $\xi = x - v_g t$, where v_g is the laser pulse group velocity. The phase velocity $v_{\rm ph}$ of the wakefield equals the group velocity of the laser pulse. In the moving frame $\xi = x - v_g t$ of the laser-pulse group velocity v_g, we have the following motion integrals:[17,23]

$$H - \beta_{\rm ph} P_x = h_0, \quad \text{and} \quad P_\perp = P_{\perp 0}\,, \qquad (3)$$

where P_x and $P_\perp$ are the longitudinal and transverse components of canonical momentum, $\beta_{\rm ph} = v_{\rm ph}/c$ is the normalized phase velocity, the integral constants h_0 and $P_{\perp 0}$ are determined by the initial state of the electron. The electron transverse, or quiver, momentum in the laser pulse is $p_\perp = a$ during the laser-plasma interactions, and the initial transverse momentum can be safely neglected. Accordingly, the Hamiltonian of the electron is

$$h(\xi, p_x) = \sqrt{1 + p_x^2 + a^2(\xi)} - \phi(\xi) - \beta_{\rm ph} p_x\,. \qquad (4)$$

From the initial conditions, the Hamiltonian is $h = h_0 = \sqrt{1 + p_{x0}^2} - \beta_{\rm ph} p_{x0}$, where p_{x0} is the initial longitudinal momentum. The longitudinal momentum of the electron according to Eq. (4) can be written as

$$p_x = \frac{\beta_{\rm ph}(\phi + h_0) \pm \sqrt{(\phi + h_0)^2 - (1 - \beta_{\rm ph}^2)(1 + a^2)}}{1 - \beta_{\rm ph}^2}\,. \qquad (5)$$

The electrostatic potential ϕ is given by the Poisson's equation[5,24]

$$\frac{\partial^2 \phi}{\partial \xi^2} = k_p^2 \gamma_{\rm ph}^2 \Big(\beta_{\rm ph} \frac{\gamma_{\rm ph}(1+\phi)}{\sqrt{\gamma_{\rm ph}^2 (1+\phi)^2 - (1 + a^2)}} - 1 \Big)\,, \qquad (6)$$

where $\gamma_{\rm ph} = 1/\sqrt{1 - \beta_{\rm ph}^2}$, $k_p = \omega_p/c$, $\xi = \xi/\lambda_L$, ω_p is the plasma frequency, and λ_L is the laser wavelength. For most practical applications, We shall consider a Gaussian laser pulse propagating in the plasma, which is written as

$$a = a_0 \exp\Big(- \frac{\xi^2}{2L_L^2} \Big) \cos(2\pi\xi)\,, \qquad (7)$$

where a_0 is the amplitude of the normalized vector potential and L_L is the pulse length. The group velocity of the relativistically strong laser pulse is given by

$$v_g \simeq c \sqrt{1 - \frac{n_e}{n_c (1 + a_0^2)^{1/2}}}\,, \qquad (8)$$

where n_e is the electron plasma density and $n_c = m\omega^2/(4\pi e^2)$ is the critical density.

2.2 *Numerical Results*

Using Eqs. (5)–(8), one can follow the motion of a plasma electron under the action of the laser pulse and its wakefield. Figure 1(a) shows the vector potential of the laser pulse and the generated scalar potential of the wake. The scalar potential minimum corresponds to the node of the plasma wave. Under this field, Fig. 1(b) shows the phase space of two typical electrons, with initial momentums $p_{x0} = 0$ and $p_{x0} = 0.2mc$, given by the solid and dashed curves, respectively. The physical parameters are $a_0 = 5$, $L_L = 5\lambda$, and $n_e = 0.02 n_c$. As expected, the radiation pressure pushes the electron forward in the ascending front and backward in the descending part of the laser pulse. The electrons achieve maximum momentum at the peak of the laser pulse. At the back node of the first period of the plasma wave, the electron with $p_{x0} = 0$ participates in the wake field oscillation, since its energy is too high to be trapped by the wake field in the moving frame ξ. On the other hand, the electron with $p_{x0} = 0.2mc$ is trapped and accelerated forward by the strong electrostatic field there. When the laser pulse is stopped and reflected by the solid target, the energetic electron can move forward inertially and pass through the latter.[11−12] In fact, one can expect that all electrons trapped in the wake plasma wave will escape in this manner.

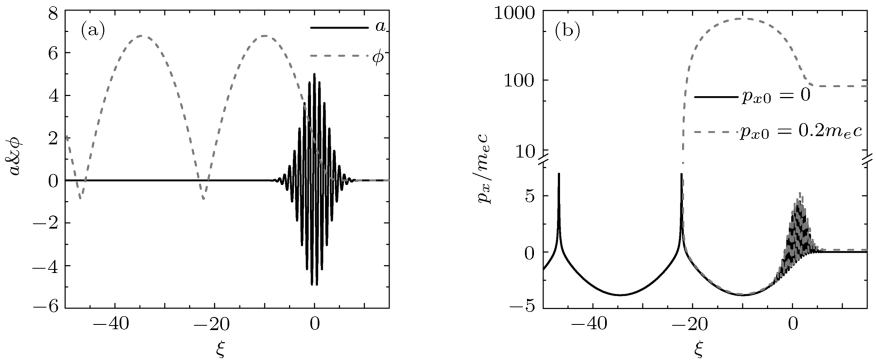

Fig. 1 (a) The vector potential a (solid curve) of the laser pulse and scalar potential ϕ (dashed curve); (b) Longitudinal electron momentum in the phase space (ξ, p_x) for two electrons, one with initial momentum $p_{x0} = 0$ (solid curve) and the other with $p_{x0} = 0.2mc$ (dashed curve), as obtained from the 1D model. The laser pulse is centered at $\xi = 0$. The physical parameters: $a_0 = 5$, $L_L = 5\lambda$, and $n_e = 0.02n_c$.

3 PIC Simulations

3.1 *Simulation Parameters*

We shall carry out 2D3V PIC simulations to demonstrate the proposed scheme using the VORPAL code.[25] A bi-Gaussian laser pulse with $\lambda = 1$ μm, a_0 =20, $L_L = 5$ μm, and spot size $w = 6$ μm is incident normally onto the plasma. The laser is linearly polarized along the y direction propagating along the x direction. The density of solid targets varies from $10n_c$ to $40n_c$ and its width is 1 μm. The density of the preplasma is between $0.005n_c$ and $0.1n_c$ and its width is 50 μm. The critical density n_c is about 1.1×10^{21} cm^{-3} for $\lambda = 1$ μm. The simulation box is 120×50 μm^2 with a grid of 3600×1000 cells. The preplasma initially occupies a region between $x = 20$ μm and $x = 70$ μm. The target is from $x = 70$ μm to $x = 71$ μm. The ion to electron mass ratio is $m_i/m_e = 1836$. The initial electron and ion temperatures are assumed to be so small that their effects can be ignored. The transverse and longitudinal boundary conditions are periodic and absorbing, respectively.

3.2 *Simulation results*

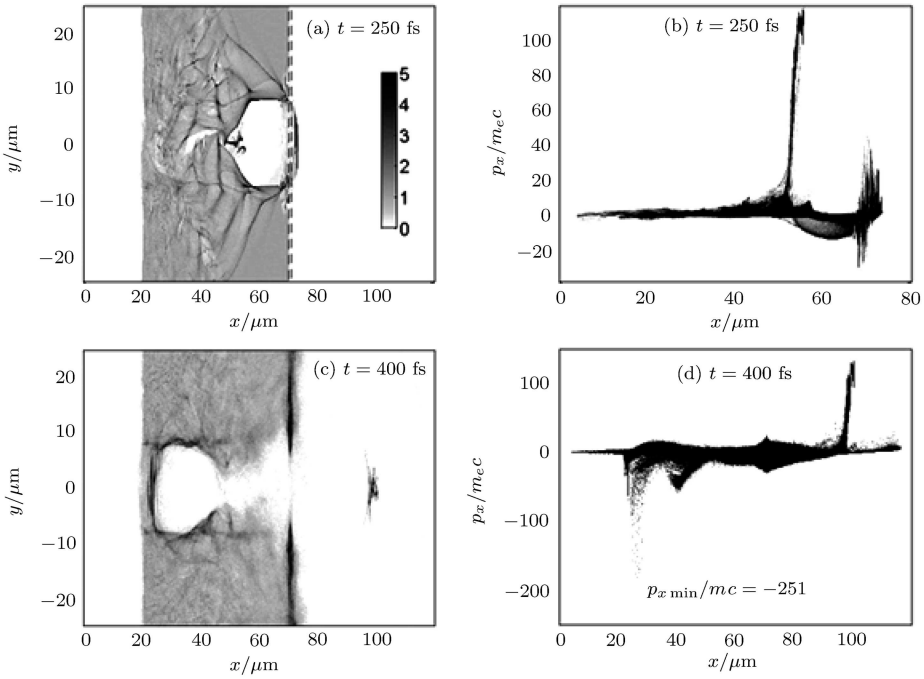

Fig. 2 The preplasma electron density and the longitudinal electron momentum at [(a) and (b)] $t = 250$ fs and [(c) and (d)] $t = 400$ fs, respectively. The dashed lines in (a) mark the edges of the target. The peak amplitude and length of the laser pulse are $a_0 = 20$ and $L_L = 5$ μm, and its spot size is 6 μm. The densities of preplasma and target are $0.02n_c$ and $30n_c$, respectively.

Figures 2(a) and 2(b) show the electron density profile and the phase space of the longitudinal electron momentum at $t = 250$ fs, when the center of the laser pulse has just arrived at the front surface of the target. One can see that an electron-free bubble is formed behind the laser pulse in the preplasma, and at the back of the bubble some electrons are trapped in the axis region. They are accelerated forward to very high energy. When the front part of the pulse is being stopped and reflected by the target, electrons there move forward inertially and then avoid the deceleration phase without much energy loss. One can also see that the electrons laterally expelled by the transverse ponderomotive force form the thin dense sheath of the bubble. The electrons in the sheath with negative momentum cover the entire bubble. When the electrons from the sheath during the wave breaking slip into the bubble, they are trapped and injected into the acceleration phase. One can see from Fig. 2(b) that the trapped electron bunch near the node of the bubble are accelerated forward monoenergetically and gain very high energy. Figure 2(c) is for $t = 400$ fs, after the laser pulse has reflected. It is shown that the energetic electron bunch in the bubble is unaffected by the reflected laser pulse and passes through the target with narrow emittance before it expands by the Coulomb explosion. When the reflected laser pulse propagates backward into the preplasma, one can see from Fig. 2(d) that it violently accelerates a small number of the return-current electrons, which of the maximum momentum in absolute value is nearly two times that of the forward ones in the backside vacuum. Note that the bubble created by the reflected pulse is open on its backside and long living. The energy spectrum of the electrons in the preplasma as well as the target at $t = 250$ fs and 400 fs is shown in Fig. 3. The narrow spike with a peak energy of 54 MeV at $t = 250$ fs is due to the trapped electron bunch in the bubble. At $t = 400$ fs, after the electron bunch has passed through the target, one can see that these electrons have been further accelerated (peak energy is now 58 MeV), and the energy spike remains narrow.

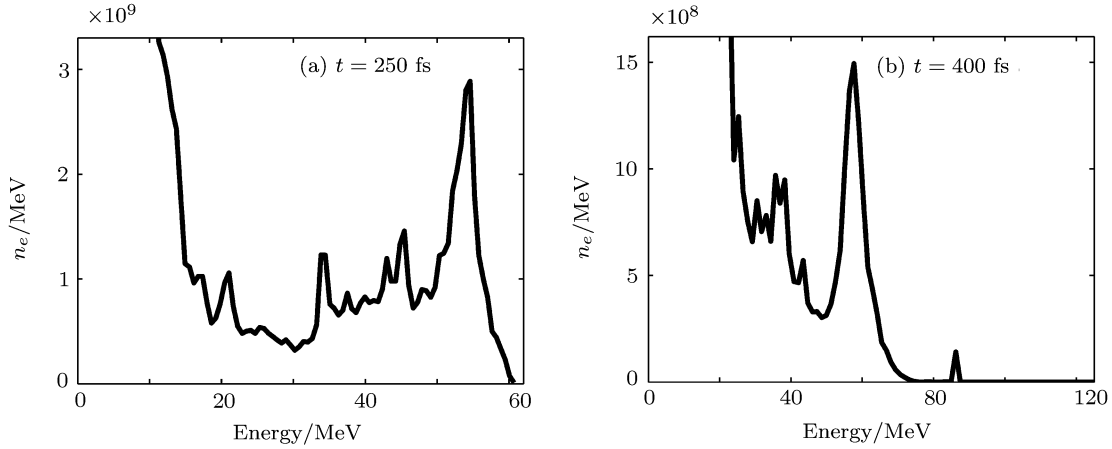

Fig. 3 The energy spectrum of the electrons at (a) $t = 250$ fs and (b) $t = 400$ fs, respectively. The parameters are the same as given in Fig. 2.

3.3 *Effects of Preplasma Density on Electron Accleration*

We have also looked into the effect of the preplasma density on electron acceleration and bunch generation. Figure 4 shows the electron density profiles at $t = 400$ fs for different preplasma densities, which are $0.005n_c$, $0.01n_c$, $0.05n_c$, and $0.1n_c$, respectively. In the lower density preplasma, $n_e = 0.005n_c$, one can see in Fig. 4(a) that the electrons trapped at the bubble back during the wave breaking can not be confined on the x axis. There are two electron bunches on the backside vacuum, which are from the up and down rims of the bubble. The radius R of the bubble scales with the laser intensity a_0 and the density n_e,[14] i.e., $R/\lambda \simeq \sqrt{a_0/(n_e/n_c)}/\pi$. It takes the electrons in the sheath more time to arrive at the base of the bubble compared with the case of higher density. According to Eqs. (8), the bubble is collapsed earlier by the reflected pulse due to the lower density. Therefore, the transverse electrostatic field is not so strong enough to drive and confine the electrons from the bubble sheath on the x axis. In the moderate density preplasma with $n_e = 0.01n_c$, although an electron bunch with density about $6n_c$ is seen to be ejected from the traget, it is not compressed efficiently in longitudinal direction compared to the result of Fig. 2(c). When the density of the preplasma increases further, there is no pronounced an electron bunch on the backside of the target, as shown in Figs. 4(c) and 4(d). One can see the electrons locate inside a wide region on the backside of the target. This is because there are parametric instabilities such as stimulated Raman scattering and two-plasmaon decay for higher densities, which can destroy the formation of the bubble and the electron bunch.

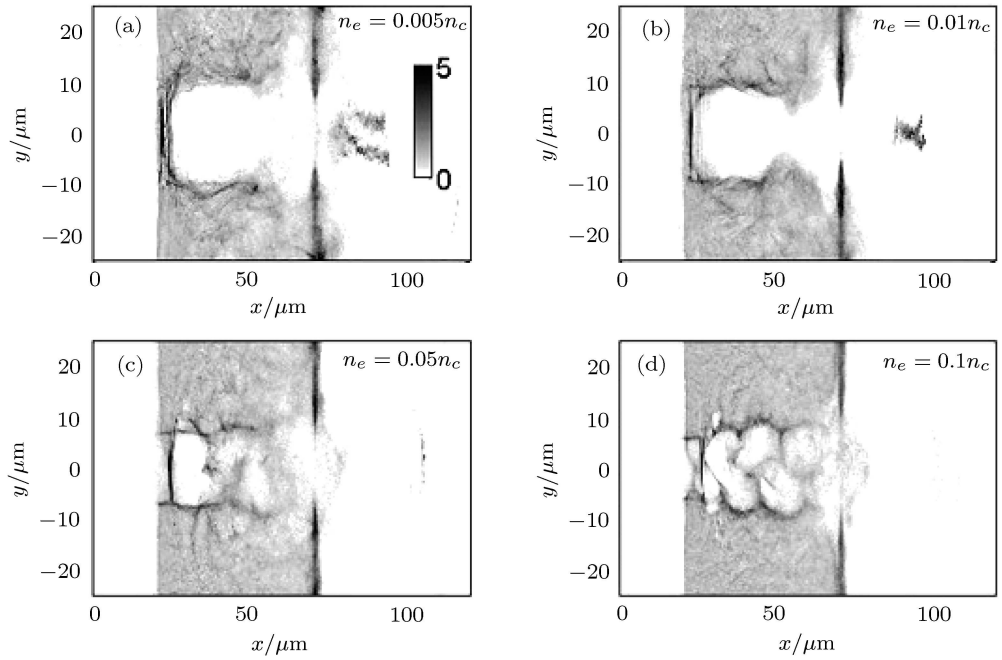

Fig. 4 The distribution of the preplasma electron density in the (x, y) plane at $t = 400$ fs: (a) $n_e = 0.005n_c$, (b) $n_e = 0.01n_c$, (c) $n_e = 0.05n_c$, and (d) $n_e = 0.1n_c$. The other parameters are the same as in Fig. 2.

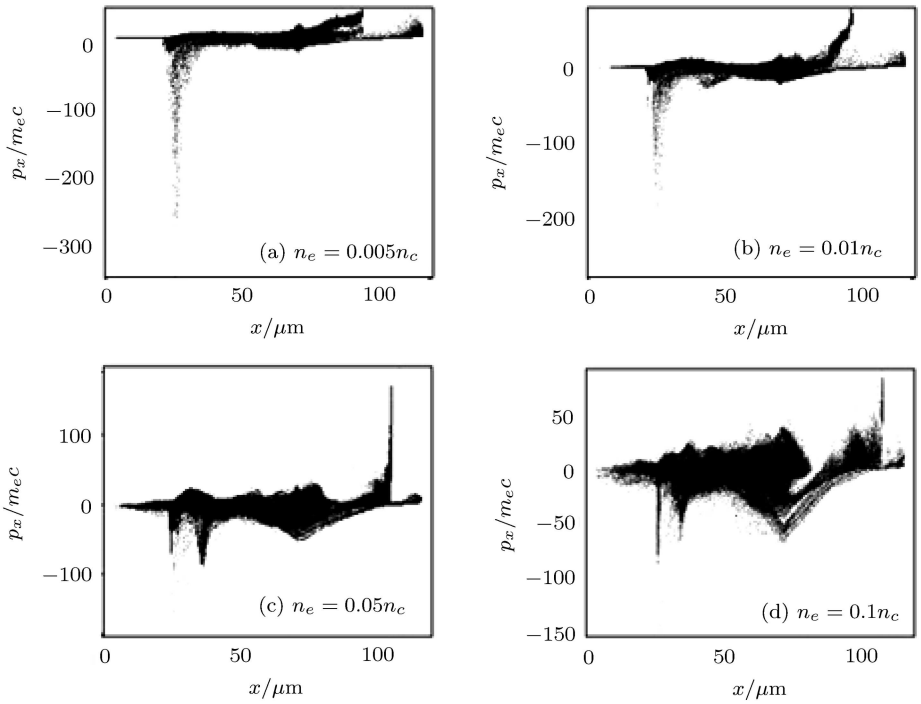

Fig. 5 The longitudinal electron momentum in the phase space (x, p_x) with different densities at $t = 400$ fs: (a) $n_e = 0.005n_c$, (b) $n_e = 0.01n_c$, (c) $n_e = 0.05n_c$, and (d) $n_e = 0.1n_c$. The other parameters are the same as in Fig. 2.

Figure 5 shows the distributions of the longitudinal electron momentum at $t = 400$ fs for the same parameters as in Fig. 4. The electrons trapped at the back of the bubble from the sheath can not be accelerated effectively forward due to deviating from the x axis as shown in Fig. 5(a). One can see from Fig. 5(b) that the velocity of the electron bunch scales linearly with the distance from the target, where for $n_e = 0.02n_c$ there is a momenta flattening in phase space as seen in Fig. 2(d), which manifests the generation of monoenergetic electrons. In the relatively high density plasma, the highly energetic electrons on the backside vacuum are accelerated directly by the ponderomotive force of the propagating laser pulse and escape from the pulse as well as the tar-

get, as shown in Figs. 5(c) and 5(d). One can also see that the momentum in absolute value of the backward accelerated electrons by the reflected laser pulse is in inverse proportion to the plasma density. According to $p_x \simeq (1+a^2)/2(\sqrt{1+p_{x0}^2}+p_{x0})$, the momentum p_x of the electron depends mainly on the initial momentum p_{x0} for a given laser pulse.[11] The lower the density is, the lager the momentum p_{x0} in absolute value of the return-current electrons is before the reflected pulse catches them. Figure 6 shows the energy spectra of the electrons at $t = 400$ fs. The parameters are the same as in Fig. 4.

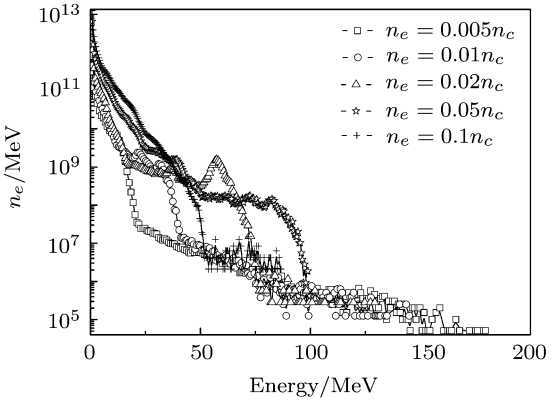

Fig. 6 The energy spectra of the electrons for different densities at $t = 400$ fs. The other parameters are the same as in Fig. 2.

The electron density $n_e = 0.02n_c$ is anticipated to be optimum for the generation of the monoenergetic electron bunch. As expected, the maximum energy of the electrons attributes to the strong backward acceleration by the reflected pulse. The lower the density is, the higher the energy maximum of the electrons is, as shown in Fig. 6.

4 Conclusion

In summary, we have investigated electron acceleration and bunch generation in the interaction between an intense femtosecond laser pulse and a target with a low-density preplasma. The preplasma electrons facing the laser pulse can be trapped and accelerated forward by the front of the pulse as well as by the intense electrostatic field at the back of the bubble. When the laser pulse is reflected by the solid target, the forward accelerated electrons in the pulse front pass inertially through it with little energy loss and scattering. It is found that the monoenergetic electron bunch in the bubble is neither affected by the pulse reflection nor by the thin target. They appear at the back of the latter as a narrow energetic bunch with small energy spread and emittance. The energy gain by the electrons in the bubble is many times that in the pulse. We have also investigated the effect of preplasma density on electron acceleration. There is an optimal preplasma density for the generation of monoenergetic electron bunch. For $I\lambda^2 = 5.48\times10^{20}$ W/cm$^2\mu$m^2 in the proposed model, the density is $n_e = 0.02n_c$ and the peak energy of the bunch is 58 MeV. The maximum electron energy is inverse proportion to the preplasma density. One can also increase the energy of the electron bunch by increasing the length of the low-density preplasma or by letting the laser pulse propagate in a long rarefied plasma channel and then stop it by a thin solid target.

Acknowledgments

The authors would like to thank Dr. Hong-Yu Wang for his contributions to the computational technique.

References

[1] T. Tajima and J.M. Dawson, Phys. Rev. Lett. **43** (1979) 267.
[2] P. Sprangle, *et al.*, Appl. Phys. Lett. **53** (1988) 2146.
[3] Y. Sentoku, *et al.*, Phys. Plasmas **5** (1998) 4366.
[4] M. Tabak, *et al.*, Phys. Plasmas **1** (1994) 1626.
[5] P. Gibbon, *Short Pulse Laser Interactions with Matter: An Introduction*, Imperial College Press, London (2005).
[6] F. He, *et al.*, Commun. Theor. Phys. **43** (2004) 910.
[7] C.T. Zhou, X.T. He, and M.Y. Yu, Appl. Phys. Lett. **92** (2008) 071502.
[8] B.S. Xie and X.T. Yin, Commun. Theor. Phys. **49** (2008) 753.
[9] B.S. Xie and H.C. Wu, Commun. Theor. Phys. **51** (2009) 1125.
[10] M.P. Liu, *et al.*, Phys. Plasmas **16** (2009) 083104.
[11] W. Yu, *et al.*, Phys. Rev. Lett. **85** (2000) 570.
[12] Y. Yin, *et al.*, Phys. Scr. **67** (2003) 544.
[13] A. Pukhov and J. Meyer-ter vehn, Appl. Phys. B **74** (2002) 355.
[14] W. Lu, *et al.*, Phys. Rev. Lett. **96** (2006) 165002.
[15] B.S. Xie, *et al.*, Phys. Plasmas **14** (2007) 073103.
[16] B. Shen, *et al.*, Phys. Plasmas **14** (2007) 053115.
[17] S.V. Bulanov, *et al.*, Plasma Phys. Rep. **32** (2006) 263.
[18] S.P.D. Mangles, *et al.*, Nature (London) **431** (2004) 535.
[19] C.G.R. Geddes, *et al.*, Nature (London) **431** (2004) 538.
[20] J. Faure, *et al.*, Nature (London) **431** (2004) 541.
[21] S. Gordienko and A. Pukhov, Phys. Plasmas **12** (2005) 043109.
[22] K. Adumi, *et al.*, Phys. Plasmas **11** (2004) 3721.
[23] T. Esirkepov, *et al.*, Phys. Rev. Lett. **96** (2006) 014803.
[24] E. Esarey and M. Pilloff, Phys. Plasmas **2** (1995) 1432.
[25] C. Nieter and J.R. Cary, J. Comput. Phys. **196** (2004) 448.